IEEE International Conference on Robotics and Automation
Minneapolis, Minnesota, April 22-28, 1996.

A Coarse-Fine Approach to Force-Reflecting Hand Controller Design

L. Stocco and S. E. Salcudean

Department of Electrical Engineering
The University of British Columbia
Vancouver, British Columbia, Canada V6T 1Z4

Abstract

A coarse-fine approach to the design of high fidelity haptic interfaces is proposed based on prior work and new psychophysics studies. The approach involves a fine-motion six-degree-of-freedom parallel Lorentz actuator mounted on a series/parallel coarse-motion stage and coupled through a compliant transmission. The frequency response of a simplified model is used to illustrate the advantages of the approach. The workspaces of three coarse-motion platforms are compared. A novel twin-elbow manipulator with all but one of the drive motors in the base is proposed for its simplicity and large workspace size.

1 Introduction

Since its early use in remote manipulation of radioactive materials, the field of teleoperation has expanded its scope to include manipulation at different scales and in virtual worlds. Applications are expected in space and undersea exploration and servicing, forestry and mining, microsurgery and microassembly, and computer-user interfaces.

The goal of teleoperation is to achieve "transparency" by mimicking human motor and sensory functions. Within the relatively narrow scope of manipulating a tool, transparency is achieved if the operator cannot distinguish between maneuvering the master controller and maneuvering the actual tool. The ability of a teleoperation system to provide "transparency" depends largely on the performance of the master. Ideally, the master should be able to emulate any environment encountered by the tool, from free-space to infinitely stiff obstacles.

It has been argued that the range of impedances that can be emulated by a teleoperation master only needs to span what can be felt by the human hand [3],[8],[9],[18],[34] [39]. This range is still being defined by ongoing human-factors and psychophysics studies [11],[18],[34],[39]. Meanwhile, specifications for a "universal" force-reflecting hand controller have been suggested by Brooks [3], Fischer [8], Lawrence [18] and Sharpe [34] who base their recommendations on surveys of telerobotic experts and literature, the relative merits of existing teleoperation systems, mathematical models and human-factors and psychophysical experiments.

Many attempts have been made to design a realistic force-reflecting master hand controller. In [5] a 6-DOF device combining three 2-DOF linkages is presented. Iwata [12] built a 9-DOF device that provides 6-DOF motion to the hand and 1-DOF motion to 3 sets of fingers. Iwata [13] also experimented with a 6-DOF haptic pen positioned by two 3-DOF manipulators. In [19] a 6-DOF joystick with three parallel pantograph linkages is reported. In [39] a hand controller using three prismatic actuators for translation and three rotary actuators for orientation is presented. In [21] a haptic probe with three active translational degrees of freedom and three passive rotational degrees of freedom is described. A 4-DOF device using only rotary actuators is presented in [17]. A 4-DOF (3 translational, 1 rotational) joystick is described in [23]. A 2-DOF five-bar linkage with a horizontal planar workspace is optimized in [9]. In [15] a linear voice coil actuated 2-DOF planar positioning device is presented. Finally, Vertut [36] presents a historical survey of earlier hand controllers, articulated arms, and exoskeletons.

The advantages of using Lorentz magnetic levitation (maglev) [10] in the design of force-feedback hand controllers have been shown in [29]. They include small mass, high frequency response, backdriveability, and low friction. Experimental results with a teleoperation system using maglev master and slave wrists have shown good transparency for small motions [30]. The main drawback encountered was the small motion range of the magnetically levitated flotor. In response to this problem, it was suggested that the maglev device be mounted on an additional 6-DOF motion stage to provide coarse positioning. In this paper, this coarse-fine approach to haptic interface design is explored further.

In Section 2, specifications collected from the literature and new psychophysics studies are used to determine design guidelines and tentative specifications. Section 3 presents evidence that a performance benefit can be realized from a dual-stage mechanism. It is also shown that the use of a compliant transmission to sum coarse and fine actuator forces in parallel mechanisms [25] can also be applied to serial mechanisms. Section 4 compares three mechanisms for the coarse-stage. One of them, a novel "twin-elbow" redundant manipulator with all but one of the actuators in the base, is selected due to its simplicity and large non-singular workspace. Section 5 presents conclusions and plans for optimization of the design parameters.

2 Performance Objectives

A literature survey that suggests design goals for a haptic interface is summarized in Table 1. By comparison, the performance figures for the maglev joystick reported in [29],[30] are shown in Table 2. These figures do, however, vary with the size of the specific device, with the force to mass ratio deteriorating slightly with scale [31].

Table 1: Reported Goals and Specifications

Design Parameter	Proposal	
Translation Range (mm)	[8] : 6.7 (x,y,z axis)✻✺ [12] : 300 (x,y,z axis)† [15] : 17 (x,y axis)† [15] : 40 (x,y axis)✻ [17] : 200 (x,y,z axis)† [21] : 250 x 170 x 80 (x,y,z axis)† [22] : 203 x 203 x 89 (x,y,z axis)✺ [27] : 160 x 100 (x,y axis)† [35] : 130-195 x 100-150 (x,y axis)✺	
Rotation Range	[4] : 99˚/ -90˚ (x axis)✺ [4] : 113˚/ -77˚ (y axis)✺ [4] : 47˚/ -27˚ (z axis)✺ [6] : ±84˚ x ±30˚(x,z axis)✺ [8] : ±30˚ (x,y,z axis)✻✺ [17] : ±86˚ (z axis)† [22] : ±45˚ (z axis)✺	
Position Bandwidth (Hz)	[3] : 3.9-9.7✻ [8] : 50✻✺	[34] : 5-10✺ [39] : 70✺
Max. Force (N)	[8] : 100✻✺ [12] : 22.6† [13] : 0.5† [15] : 6.3† [17] : 12†	[21] : 10† [22] : 44.48✺ [27] : 10† [38] : 151- 463✺
Max. Torque (Nm)	[1] : 1.26✺ [2] : 9.925✺ [12] : 0.294†	[17] : 0.4† [22] : 1.356✺ [38] : 0.658✺
Force/Torque Bandwidth (Hz)	[3] : 320✺ [9] : 300✻ [11] : 450✺	[15] : 1000† [34] : 300✺ [36] : 100✺
Max. Velocity (m/s)	[3] : 1.1✻	[8] : 1✻✺
Max. Accel. (m/s^2)	[3] : 12.2✻	[8] : 9.81✻✺
Min. Nat. Freq. (Hz)	[23] : 100 Hz†	

✺*Based on psychophysics and/or human-factors studies.*
✻*Based on experience with existing haptic interfaces.*
†*Reported capability of an existing haptic interface.*

The results show that the consensus figures for an adequate workspace exceed what can be achieved with a single-stage maglev device since it would be extremely difficult, if not impossible, to increase the workspace by an order of magnitude. Although the results also show that the continuous maximum forces generated by the maglev device only marginally satisfy the quoted requirements, the frequency response specifications (assuming they apply to the motion travel accommodated by maglev devices) are far in excess of the quoted requirements. The implications of the above comparison are discussed below.

Table 2: Maglev Joystick Characteristics

Characteristic	Specification
Cylindrical Diameter Height	13 cm 11 cm
Nominal Translational Motion Range Nominal Rotation Motion Range	± 4.5 mm ± 7˚
Flotor Mass	0.650 Kg
Closed-Loop Translational Bandwidth Closed-Loop Rotational Bandwidth	> 30 Hz > 15 Hz
Position Resolution	1 µm
Force Bandwidth[A]	> 1000 Hz
Force Resolution[B]	0.1 N
Maximum Continuous Force[C]	18 N
Peak Force[C,D]	60 N
Maximum Continuous Torque[C,D]	0.6 Nm
Peak Torque[C,D]	6 Nm
Peak Acceleration[C]	90 m/s^2

A. Based on coil time constant.
B. Digital-to-analog converter dependent.
C. Axial or z-axis force: x, y axes forces roughly 30% smaller.
D. Coil amplifier dependent.

2.1 Workspace Limitation

As suggested in [10],[29] the severe workspace limitation of a maglev device could be overcome by mounting it on a 6-DOF coarse positioning stage which would track the maglev flotor held by the operator. This arrangement presents a clear design trade-off between the coarse-stage and fine-stage performance requirements. A maglev device with a small workspace can produce large forces but also would place large demands on the tracking ability of the coarse-stage. To select the optimum maglev device workspace, it is necessary to understand the kind of operator hand motions that can be expected for a pencil-like grip as envisaged.

It is difficult to determine from prior studies how significantly the maximum motion frequency of the human hand drops with amplitude. It was therefore determined experimentally by asking ten subjects to make pencil strokes varying in width from 1.5 to 160 mm as quickly as possible. A position tracking device (Bird™ magnetic sensor) was mounted to the tip of the index finger of each subject to record the hand trajectories. The trajectories were then analyzed to pick out the highest dominant frequency component. The average results, that include the best of three repeated trials for each subject, are shown in Figure 1 with the standard deviation ranging between 0.6 and 1.4.

The results show that the maximum motion frequency that humans can generate does not drop significantly (~ 0.7

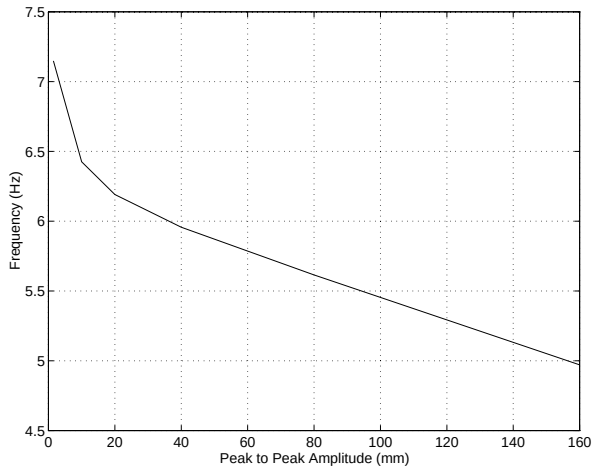

Figure 1: Maximum Motion Frequency vs. Amplitude

Hz) with amplitude in the range of motion (0 - 20 mm) that can be accomplished by a reasonably sized single-stage maglev device. The coarse-stage must therefore be able to track motions of up to about 7 Hz since there is little to be gained by enlarging the maglev's motion range at the expense of force.

2.2 Force Limitation

Although the continuous force limitation of a maglev device may limit the maximum static stiffness it can emulate, its ability to emulate contact with stiff walls is enhanced by its high acceleration. This is demonstrated in [32] where ten subjects were asked to move a maglev joystick against a virtual wall and press a button upon detecting it. The surface models used were a simple spring with stiffnesses ranging from 1 to 10 N/mm and the same spring with a braking force added that brings the joystick to rest within a single control sample upon penetration. This corresponds to accelerations of up to 90 m/s^2. The results showed that subjects could locate the wall more accurately and with less penetration when the braking pulse was added and that performances did not improve significantly when stiffnesses exceeded 6-7 N/mm.

An analysis of the data using ANOVA tables and F-ratios showed that both increased stiffness and acceleration significantly decrease wall penetration and increase the accuracy with which the wall can be located, with minimal interaction between the two. Consequently for stiff wall emulation, the maximum force exerted by the haptic interface is no more important than its maximum acceleration. Therefore, in view of the high acceleration capability of a maglev device, the lack of large continuous forces capabilities may not be a debilitating factor.

In the next section it is shown that the coarse-fine approach used to enlarge the workspace of a maglev device can also be used to increase its maximum force by means of a compliant transmission.

3 Effect of Compliant Transmission

Morrell & Salisbury [25] argue that the high force resolution and bandwidth of a micro actuator acting on a load can be augmented by the high force capability of a macro actuator by connecting the large actuator to the load via a flexible transmission. A simple model with mathematical relations showing the force acting on the load and the impedance seen by the load are presented in Figure 2. The subscripts *c*, *f*, *t* and *l* denote coarse, fine, transmission and load components, respectively, and the subscript *e* denotes system equivalents. Both macro and micro actuators act in parallel with respect to the same mechanical ground. As opposed to the series macro-micro actuation schemes proposed in the past [16],[28],[30], [32],[33],[37], their parallel combination has the full static force capability of the macro actuator but because of the parallel connection, inherits the limited motion range of the micro actuator.

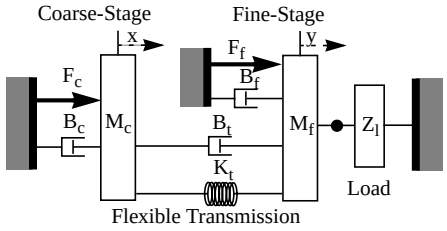

$$F_e = \frac{Z_t F_c}{Z_c + Z_t} + F_f \qquad Z_e = \frac{Z_t Z_c}{Z_c + Z_t} + Z_f$$

$$Z_c = sM_c + B_c \qquad Z_f = sM_f + B_f \qquad Z_t = B_t + \frac{K_t}{s}$$

$$\lim_{Z_t \to 0} F_e = F_f \qquad \lim_{Z_t \to 0} Z_e = Z_f$$

$$\lim_{Z_t \to \infty} F_e = F_c + F_f \qquad \lim_{Z_t \to \infty} Z_e = Z_c + Z_f$$

Figure 2: Model of Parallel Dual-Stage Device

While it is agreed that the actuators must be flexibly coupled in parallel to sum up the individual force / impedance contributions it should be pointed out that they may still be rigidly connected in series with little repercussion. This hybrid device is created by rigidly mounting the stator of the fine-stage to the flotor of the coarse-stage and flexibly coupling together the flotors of the two stages. A model similar to that in Figure 2 for the hybrid device is presented in Figure 3.

Just as in the parallel device described in [25], the force capability and internal impedance of the dual-stage device mimic that of the fine-stage for a compliant transmission and approach that of the coarse-stage as the transmission is made stiffer. The critical difference is that the workspace size of the hybrid device is dictated by the coarse-stage which must, however, bear the additional payload of transporting the fine-stage.

For the hybrid device, the effect of transmission impedance on the maximum force magnitude and mechanical impedance magnitude presented to the load

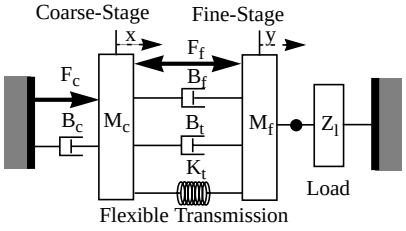

$$F_e = \frac{(Z_t + B_f)F_c + Z_c F_f}{Z_c + Z_t + B_f} \qquad Z_e = \frac{(Z_t + B_f)Z_c}{Z_c + Z_t + B_f} + Z_f$$

With $B_f \ll |Z_c|$ $\lim_{Z_t \to 0} F_e = F_f$ $\lim_{Z_t \to 0} Z_e = Z_f$

$\lim_{Z_t \to \infty} F_e = F_c$ $\lim_{Z_t \to \infty} Z_e = Z_c + Z_f$

Figure 3: Model of Hybrid Dual-Stage Device

over a range of frequencies is illustrated in Figure 4 and Figure 5 respectively. The transmission impedance $B_t + K_t s^{-1}$ is selected by varying K_t and selecting B_t such that the transmission supporting the fine-stage mass is critically damped:

$$\frac{1}{s^2 M_f + sB_t + K_t} = \frac{1}{s^2 + 2\zeta\omega_0 s + \omega_0^2}, \zeta = 1$$

F_f, M_f and B_f refer to the fine-stage force, mass and damping respectively and are assigned values similar to those of the maglev device described in Table 2. F_c, M_c and B_c refer to the coarse-stage force, mass and damping respectively and are assigned the typical values $F_c = 10F_f$, $M_c = 50M_f$ and $B_c = 1000B_f$.

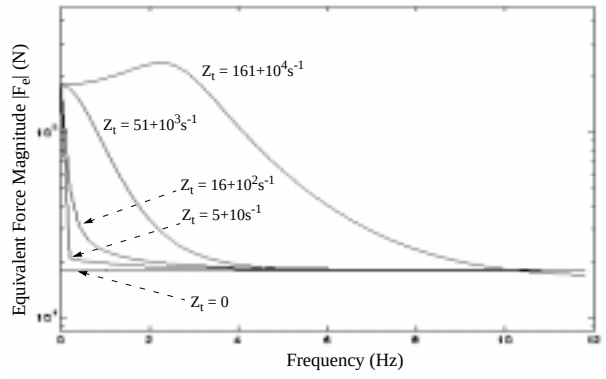

Figure 4: Equivalent Force

4 Proposed Coarse-Stage

As discussed in Section 2, the large motion frequency response of the coarse-stage must be as high as 7 Hz. Since this would be difficult to achieve with a purely serial mechanism, only mechanisms with some parallel actuation are considered. In this section, three candidates are compared in terms of their complexity and workspace; a prismatically actuated "Stewart" platform [7], a five-bar linkage actuated "Spider" platform [24], and a novel series/parallel mechanism called the "Twin-Elbow"

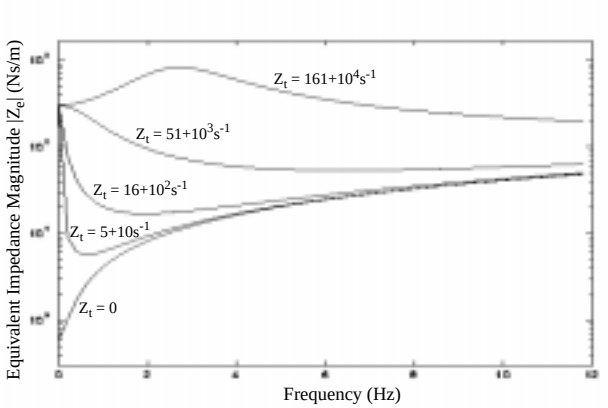

Figure 5: Equivalent Impedance

platform. Diagrams of these three mechanisms with geometry assignments are shown in Figure 6 through Figure 8.

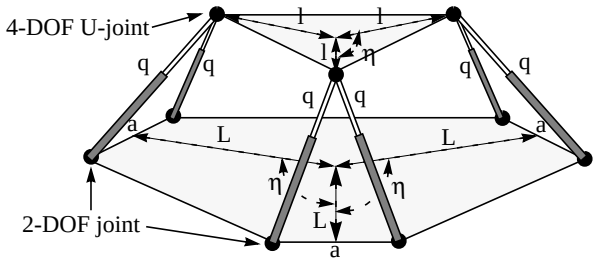

Figure 6: Diagram of Stewart Platform

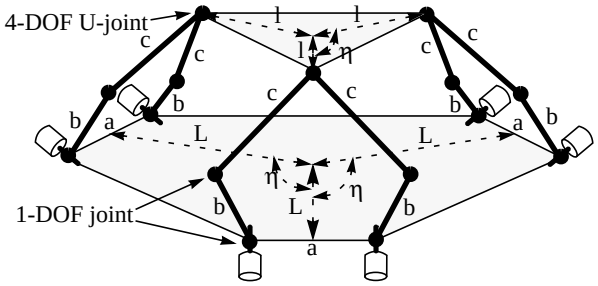

Figure 7: Diagram of Spider Platform

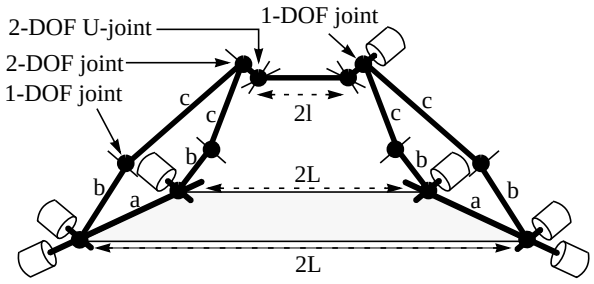

Figure 8: Diagram of Twin-Elbow Platform

The twin-elbow platform is a 5-DOF series/parallel platform with a 1-DOF "wrist" mounted in series to its platform. It is similar to Iwata's design which combines two 3-DOF parallelogram linkage robots to position a 6-

DOF haptic pen [13]. The twin-elbow platform has eleven fewer passive revolute joints and one fewer U-joint than either of the other two platforms resulting in less friction and backlash. There is, however, a significant inertial contribution from the wrist actuator but it is partially offset by having two fewer base to platform linkages. By actuating and sensing the folding or "waist" axis of each five-bar linkage, a platform singularity is eliminated and the kinematics of the platform are highly simplified. The singularity that is eliminated occurs when the tips of the two five-bar linkages both lie in the plane of the five-bar linkage with a passive waist[1].

As its name suggests, the twin-elbow platform is equivalent to two elbow manipulator arms with passive spherical wrists joined at their distal ends through an actuator aligned with the wrist centers. The inverse and direct kinematics of this mechanism are easily computed and are not described here. It can also be shown that the singular configurations of the twin-elbow platform occur when and only when (i) either of the five-bar linkages is in a singular configuration (see Figure 9, #1, #2), (ii) the tip of a five-bar linkage intersects the axis of the five-bar linkage waist (see Figure 9, #3, #4), (iii) either of the five-bar linkages is at its workspace limit or (iv) the tips of the five-bar linkages align with a forearm of either five-bar linkage (this corresponds to a spherical wrist singularity).

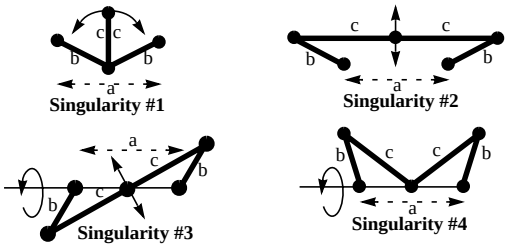

Figure 9: Singular Positions of Waist and Shoulder Actuated Five-Bar Linkage

The five-bar linkage singularities are not particularly problematic since, by design, singularity #1 is eliminated if $a > 2b$, and singularities #2, #3 and #4 are eliminated if $c > (b + a/2)$. Since the workspace is maximized when $c \approx b$ it is best to impose $c > (b + a/2)$ and maintain an elbow out constraint to eliminate singularity #1.

In the following, a comparison between the workspaces of the three candidates are presented. For a fair comparison, the mechanisms were sized to have similar footprints and favorable geometries. For the Stewart platform, an optimization of the Jacobian matrix carried out in [18] suggests triangles for the base and platform, with a 2:1 base to platform ratio. With the link lengths approximated from the vertical range presented in [18], the resulting geometry is tabulated in Table 3 where q_{min} and q_{max} refer to the minimum and maximum possible lengths of the Stewart platform's prismatic actuators.

Next, parameters for the spider platform were chosen to make it similar to the Stewart platform. Links *b* and *c* were selected to add up to q_{max} and were made similar in length to achieve good range while maintaining $c > (b + a/2)$ to avoid singularities. The platform remains identical but the base could not be made triangular as a high degree of linkage collisions would occur in practice. The footprint is therefore kept similar but *a* is approximately halved.

The geometry of the twin-elbow platform was made identical to that of the Spider platform. Its alternative architecture is its only distinction.

Table 3: Robot Geometry[A]

Robot	q_{min}	q_{max}	a	b	c	L	l
Stewart Platform	9	18	3.5	n/a	n/a	2	1
Spider Platform	n/a	n/a	2	8	10	2	1
Twin-Elbow Platform	n/a	n/a	2	8	10	2	1

A. Notation follows Figure 6 through Figure 8.

In Figure 10, "semi-dextrous" workspaces of each of the three candidate mechanisms are displayed. A point belongs to such a semi-dextrous workspace if the mechanism end-point (the platform centroid) can be placed there and rolled, pitched and yawed ±30˚.

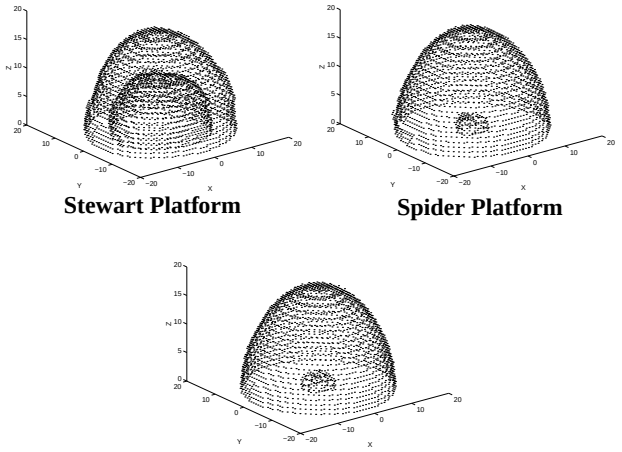

Figure 10: Example Workspaces of Candidate Robots

The spider and twin-elbow platforms have very similar workspaces which are clearly superior to that of the Stewart platform which has a large void in its centre due to the constraint of prismatic cylinders which can, at best, retract to half of their full length. The superiority of the twin-elbow over the spider becomes explicit after considering a constraint of the U-joints that join the five-bar linkages to the platforms. Due to typical physical constraints and also to avoid singular positions, the U-

1 Note that the same redundant actuation and sensing approach can be employed for the Spider platform.

joints are not allowed to exceed ±85˚. The resulting workspaces are shown in Figure 11.

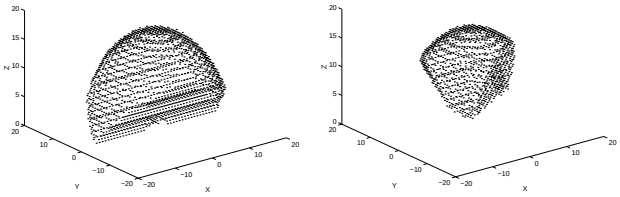

Twin-Elbow Platform **Spider Platform**

Figure 11: Example Workspaces with U-Joint Constraint

5 Conclusions and Future Work

For a force-reflecting hand controller to emulate a broad range of virtual environments with good transparency, it must have performance capabilities comparable to those of the human hand. Since the sensing ability of the human hand demands a very high bandwidth haptic device, a maglev wrist is well suited for this purpose. Unfortunately, emulation of high-impedance environments and reasonable position resolution without rate control require both a greater continuous force/torque capability as well as a workspace that is orders of magnitude larger than that offered by a maglev wrist.

In prior work, a series coarse-fine approach has been proposed to solve the workspace limitation of a maglev device. A psychophysics study presented in this paper suggests that it is not worth increasing the workspace of the maglev device at the expense of its force capability so the coarse-stage that transports it will have to achieve the full motion bandwidth demanded by the human hand. It is also argued that the force/torque capability of the maglev device can be enhanced by placing a flexible transmission such as a piece of elastic material between its flotor and stator.

Three parallel platform mechanisms are evaluated for use as a coarse-stage. Of the three, the preferred choice is a novel twin-elbow platform. This manipulator is chosen because of its simplicity, its superior workspace size and its inherent lack of singular positions which is partly brought about by actuator redundancy.

Before building a prototype, the geometry of the twin-elbow manipulator must be optimized along the lines of [9] to minimize the worst case conditioning of the Jacobian matrix within its applicable workspace which will be rectangular by design. Motors and gear ratios will be chosen to select an optimal trade-off between moving mass and available torque, velocity and acceleration.

The maglev wrist will also require optimization of its overall geometric scale, gap size and the dynamic properties of its flexible core to fine tune its maximum force/torque, workspace size and bandwidth. Finally a flexible material will have to be chosen to couple the maglev flotor and stator to optimally compromise the performance characteristics of the coarse and fine stages.

Acknowledgements

The authors would like to thank Tim Vlaar and Dan Chan for their contributions to one of the psychophysics studies. This work is supported by the Canadian IRIS Network of Centers of Excellence.

References

[1] S.D. Adams, P.J. Peterson, “Maximum Voluntary Hand Grip Torque for Circular Electrical Connectors”, Human Factors, Vol. 30, No. 6, pp. 733-745, 1988.

[2] P.A. Anderson, C.E. Chanoski, D.L. Devan, B.L. McMahon, E.P. Whelan, “Normative Study of Grip and Wrist Flexion Strength Employing a BTE Work Simulator”, The Journal of Hand Surgery, Vol. 15A, No. 3, pp. 420-425, May 1990.

[3] T.L. Brooks, “Telerobotic Response Requirements”, Proc. IEEE Int. Conf. Sys. Man Cyb. (Los Angeles, California), pp. 113-120, Nov. 4-7, 1990.

[4] D.B. Chaffin, G.B.J. Andersson, “Occupational Biomechanics”, John Wiley & Sons, 1991.

[5] K. Cleary, T. Brooks, “Kinematic Analysis of a Novel 6-DOF Parallel Manipulator”, Proc. IEEE Int. Conf. Robotics & Auto. (Atlanta, USA), pp. 708-713, May 2-6, 1993.

[6] D. Dowson, V. Wright, “An Introduction to the Bio-Mechanics of Joints and Joint Replacement”, Mechanical Engineering Publications, 1982.

[7] E.F. Fichter, “A Stewart Platform-Based Manipulator: General Theory and Practical Construction”, Int. J. Robotics Res., Vol. 5, No. 2, pp. 157-182, 1986.

[8] P. Fischer, R. Daniel, K.V. Siva, “Specification and Design of Input Devices for Teleoperation”, Proc. IEEE Int. Conf. Robotics & Auto. (Cincinnati, Ohio), pp. 540-545, May 1990.

[9] V. Hayward, J. Choksi, G. Lanvin, C. Ramstein, “Design and Multi-Objective Optimization of a Linkage for a Haptic Interface”, Proc. ARK ‘94, 4th Int. Workshop on Adv. in Robot Kin. (Ljubliana, Slovenia), June 1994.

[10] R.L. Hollis, S.E. Salcudean, P.A. Allen, “A six Degree-of-Freedom Magnetically Levitated Variable Compliance fine Motion Wrist: Design, Modelling and Control”, IEEE Trans. Robotics & Auto., vol. 7, pp. 320-332, June 1991.

[11] I. Hunter, L. Jones, T. Doukoglou, S. Lafontaine, P. Hunter, M. Sagar, “Ophthalmic Microsurgical Robot and Surgical Simulator”, Telemanipulator and Telepresence Technologies, Vol. 2351, pp. 184-190, 1994.

[12] H. Iwata, “Artificial Reality with Force-Feedback: Development of Desktop Virtual Space with Compact Master Manipulator”, SIGGRAPH (Dallas, USA), Vol. 24, No. 4, pp. 165-170, August 6-10, 1990.

[13] H. Iwata, “Pen-based Haptic Virtual Environment”, IEEE Int. Symp. Virtual Reality (Seattle, Washington), pp. 287-292, 1993.

[14] H. Kazerooni, “Human/Robot Interaction via the Transfer of Power and Information Signals Part I: Dynamics and

Control Analysis", Proc. 1989 IEEE Int. Conf. Robotics & Auto. (Scottsdale, Arizona), pp. 1632-1640, May 14-18, 1989.

[15] A.J. Kelley, S.E. Salcudean, "The Development of a Force-Feedback Mouse and its Integration into a Graphical User Interface", Proc. Int. Mech. Eng. Congress & Exposition (Chicago, USA), DSC-Vol. 55-1, pp.287-294, Nov. 6-11, 1994.

[16] O. Khatib, "Inertial Characteristics and Dextrous Dynamic Coordination of Macro/Micro-Manipulator Systems", 7th CISM-IFToMM Symp. Theory & Practice of Robots & Manipulators (Udine, Italy), Sept. 1988.

[17] T. Kotoku, K. Komoriya, K. Tanie, "A Force Display System for Virtual Environments and its Evaluation", IEEE Int. Workshop on Robot & Human Commun. (Tokyo, Japan), pp. 246-251, Sept. 1-3, 1992.

[18] D.A. Lawrence, J.D. Chapel, "Performance Trade-Offs for Hand Controller Design", Proc. IEEE Int. Conf. Robotics & Auto. (San Diego, California), pp. 3211-3216, May 1994.

[19] G.L. Long, C.L. Collins, "A Pantograph Linkage Parallel Platform Master Hand Controller for Force-Reflection", Proc. IEEE Int. Conf. Robotics & Auto. (San Diego, California), Vol. 4, pp. 3211-3216, May 9-12, 1994.

[20] O. Ma, J. Angeles, "Optimum Architecture Design of Platform Manipulators", 91 ICAR. 5th Int. Conf. Adv. Robotics (Pisa, Italy), pp. 1130-1135, June 19-22, 1991.

[21] T.H. Massie, J.K. Salisbury, "The PHANToM Haptic Interface: A Device for Probing Virtual Objects", Proc. Int. Mech. Eng. Congress & Exposition (Chicago, USA), Vol. DSC-Vol. 55-1, pp. 295-301, Nov. 6-11, 1994.

[22] P.A. Millman, J.E. Colgate, "Design of a Four Degree-of-Freedom Force-Reflecting Manipulandum with a Specified Force/Torque Workspace", Proc. IEEE Int. Conf. Robotics & Auto. (Sacramento, California), pp. 1488-1493, Apr. 9-11, 1991.

[23] P.A. Millman, M. Stanley, J.E. Colgate, "Design of a High Performance Haptic Interface to Virtual Environments", IEEE Int. Symp. Virtual Reality (Seattle, Washington), pp. 216-222, 1993.

[24] M. Mimura, Y. Funahashi, "A New Analytical System Applying 6 DOF Parallel Link Manipulator for Evaluating Motion Sensation", Nissan Technical Report, 1994.

[25] J.B. Morrell, J.K Salisbury, "In Pursuit of Dynamic Range: Using Parallel Coupled Actuators to Overcome Hardware Limitations", Proc. of 4th Int. Symp. Experimental Robotics (Stanford, California), ISER'95, pp 165-170, June 30 - July 2, 1995.

[26] G.J. Raju, G.C. Verghese, T.B. Sheridan, "Design Issues in 2-Port Network Models of Bilateral Remote Manipulation", Proc. IEEE Int. Conf. Robotics & Auto. (Scottsdale, Arizona), pp. 1316-1321, May 14-18, 1989.

[27] C. Ramstein, V. Hayward, "The PANTOGRAPH: A Large Workspace Haptic Device for a Multi-Modal Human-Computer Interaction", Proc. ACM/SIGCHI Conf. Human Factors in Computing Sys. (Boston, MA), Apr. 1994.

[28] J.R. Sagli, O. Egeland, "Dynamic Coordination and Actuator Efficiency Using Momentum Control for Macro-Micro Manipulators", Proc. IEEE Int. Conf. Robotics & Auto. (Sacramento, California), pp. 1201-1206, Apr. 9-11, 1991.

[29] S.E. Salcudean, N.M. Wong, R.L. Hollis, "A Force-Reflecting Teleoperation System with Magnetically Levitated Master and Wrist", Proc. IEEE Int. Conf. Robotics & Auto. (Nice, France), pp. 1420-1426, May 10-15, 1992.

[30] S.E. Salcudean, N.M. Wong, "Coarse-Fine Motion Coordination and Control of a Teleoperation System with Magnetically Levitated Master and Wrist", 3rd Int. Symp. Experimental Robotics (Kyoto, Japan), Oct. 28-30, 1993.

[31] S.E. Salcudean, J. Yan, "Towards a Force-Reflecting Motion-Scaling System for Microsurgery", Proc. IEEE Int. Conf. Robotics & Auto. (San Diego, California), pp. 2296-2301, May 9-12, 1994.

[32] S.E. Salcudean, T. Vlaar, "On the Emulation of Stiff Walls and Static Friction with a Magnetically Levitated Input-Output Device", Proc. Int. Mech. Eng. Congress & Exposition (Chicago, USA), Vol. DSC-Vol. 55-1, pp. 303-309, Nov. 6-11, 1994.

[33] A. Sharon, N. Hogan, D.E. Hardt, "High Bandwidth Force Regulation and Inertia Reduction Using a Macro/Micro Manipulator System", Proc. IEEE Int. Conf. Robotics & Auto. (Philadelphia, USA), pp. 126-132, Apr. 24-29, 1988.

[34] J.E.E. Sharpe, "Technical and Human Operational Requirements for Skill Transfer in Teleoperations", Int. Symp. Teleoperation & Control (Bristol, England), pp. 175-187, July, 1988.

[35] U. Tränkle, D. Deutschmann, "Factors Influencing Speed and Precision of Cursor Positioning Using a Mouse", Ergonomics, Vol. 34, No. 2, pp. 161-174, 1991.

[36] J. Vertut, "Control of Master Slave Manipulators and Force Feedback", Proc. 1977 Joint Auto. Control Conf., 1977.

[37] T. Vlaar, "Mechanism Emulation with a Magnetically Levitated Input/Output Device", Master's Thesis, University of British Columbia, Dec. 1994.

[38] W.E. Woodson, "Human Factors Design Handbook", McGraw Hill, 1981.

[39] H. Yokoi, J. Yamashita, Y. Fukui, M. Shimojo, "Development of 3D-Input Device for Virtual Surface Manipulation", 3rd IEEE Int. Workshop on Robot & Human Commun. (Nagoya, Japan), pp. 134-139, July 18-20, 1994.